https://doi.org/10.5194/wes-2022-46
Preprint. Discussion started: 31 May 2022

WIND ENERGY SCIENCE DISCUSSIONS
Open Access
european academy of wind energy

Breakdown of the velocity and turbulence in the wake of a wind turbine - Part 1: large eddy simulations study.

Erwan Jézéquel[1,2], Frederic Blondel[1], and Valery Masson[2]

[1]IFP Energies nouvelles, 1-4 Avenue de Bois Préau, Rueil-Malmaison, France
[2]Centre National de Recherches Météorologiques, 42 avenue Gaspard Coriolis, Toulouse, France

Correspondence: Erwan Jézéquel (erwan.jezequel@ifpen.fr)

Abstract. A new theoretical framework, based on wake analysis in the moving and fixed frames of reference (MFOR and FFOR), is proposed to break down the velocity and turbulence fields in the wake of a wind turbine. This approach adds theoretical support to models based on the dynamic wake meandering (DWM) and opens the way for a fully analytical and physically-based model of the wake that takes meandering and atmospheric stability into account, which is developed in the companion paper. The mean velocity and turbulence in the FFOR are broken down into different terms, which are functions of the velocity and turbulence in the MFOR. These terms can be regrouped as pure velocity, pure meandering, pure turbulence and cross-terms, the last ones being implicitly neglected in the DWM. The shape and relative importance of the different terms are estimated with the large eddy simulation solver Meso-NH coupled with an actuator line method. A single wind turbine wake is simulated on flat terrain, under three cases of stability: neutral, unstable, and stable. In the velocity breakdown, the cross-term is found to be relatively low. This is not the case for the turbulence breakdown equation where even though they are overall of a lesser magnitude than the pure terms, the cross-terms redistribute the turbulence and induce non-negligible asymmetry. It is also found that as atmospheric stability increases, the pure turbulence contribution becomes relatively larger and pure meandering relatively smaller.

1 Introduction

The wake behind a wind turbine is characterised by a decrease of wind velocity and increased turbulence compared to the inflow properties, leading respectively to a decreased generated power and increased loads for downstream turbines. The stability of the atmospheric boundary layer (ABL) influences the wake recovery (Abkar and Porté-Agel, 2015) and the large-scale eddies carried in this region of the atmosphere are often associated with wake meandering, i.e. oscillations of the instantaneous wake around its mean position (Larsen et al., 2008). This phenomenon is schematised in Fig. 1: the instantaneous wake at two different times is drawn in blue and dashed lines, and the time-averaged wake is drawn in green and continuous lines. The meandering can cause a downstream turbine to be successively outside (a) and inside (b) the wake even though on a time-averaged basis it is always fully embedded in the wake (in green in both schemes). Due to these unsteady displacements, the time-averaged wake widths will be larger and the time-averaged maximum velocity deficit lower (continuous green curve in Fig. 1) than their instantaneous counterparts (dashed blue curve in Fig. 1).

https://doi.org/10.5194/wes-2022-46
Preprint. Discussion started: 31 May 2022

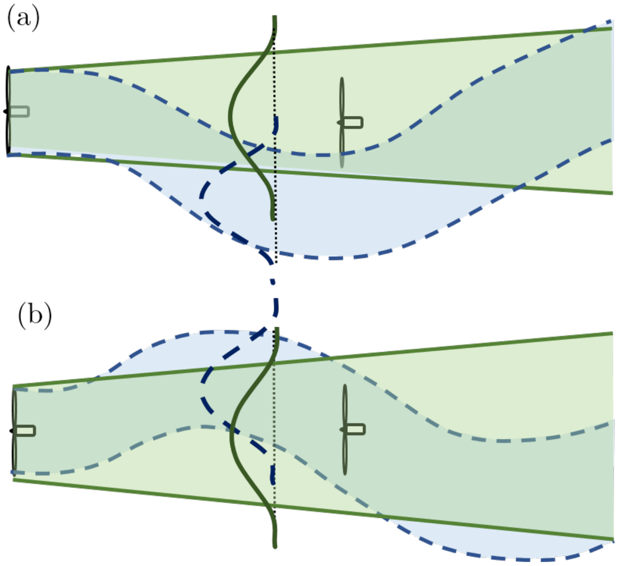

Figure 1. Schematic of the wake meandering phenomenon. The mean (continuous green curve) and instantaneous (dashed blue curve) velocity profiles are plotted at two different time steps: (a) the downstream turbine is partially outside the wake; (b) the downstream turbine is inside the wake.

The evolution of the time-averaged wake may thus be considered as the combination of two phenomena: on one hand the wake expansion and dissipation due to the turbulent diffusion and on the other hand wake meandering due to large-scale forcing of the ABL. Most analytical models are calibrated directly in the frame of reference linked to the ground (called hereafter fixed frame of reference or FFOR) against reference data averaged over the meandering time period, and the wake widths are written as a function of the turbulence intensity (TI) upstream the turbine. This approach is straightforward but the phenomena of meandering and turbulent mixing are not differentiated. The issue is that the atmospheric stability impacts meandering, leading to different time-averaged wake recoveries for a given upstream TI at hub height (Du et al., 2021). In order to model accurately wind turbine wakes in non-neutral ABL, it is proposed to calibrate independently the effect of meandering and the effect of wake expansion due to diffusion.

This can be achieved with the use of the moving frame of reference (MFOR), which is displaced with the wake centre at each time step. Due to the spreading caused by the meandering, the mean velocity deficit in the FFOR is weaker and wider compared to the mean velocity deficit in the MFOR (continuous and dashed profiles in Fig 1). Conversely, the turbulence (not shown on the scheme) is stronger in the FFOR compared to the MFOR (Larsen et al., 2019). The instantaneous streamwise velocity can be changed from one frame to another according to the relation:

$$U_{MF}(x,y,z,t) = U_{FF}(x, y + y_c(x,t), z + z_c(x,t), t) \quad (1)$$

https://doi.org/10.5194/wes-2022-46
Preprint. Discussion started: 31 May 2022

where subscripts MF and FF denote the velocity fields in the MFOR and FFOR respectively, $y_c(x,t)$ and $z_c(x,t)$ are the time series of the wake centre at the downstream position x. The concept of MFOR has originally been introduced for the dynamic wake meandering (DWM) model (Larsen et al., 2008) which aims at modelling the unsteady effects of meandering. The methodology to retrieve the velocity and turbulence fields in the FFOR with this model is briefly introduced here. In the DWM model, the wake in the MFOR is assumed to be steady and axisymmetric (Ainslie, 1985), and wake expansion and dissipation are assumed to be driven by turbulent mixing and the turbine's operating conditions. This steady wake is advected as a passive tracer by the largest eddies of the ABL to get the unsteady wake in the FFOR. If the unsteady FFOR velocity field is required, Eq. 1 is used with $U_{MF}(x,y,z,t) = U_{MF}(x,r)$ with $r = \sqrt{y^2+z^2}$ the radial component of the cylindrical system of coordinates. If only the time-averaged field is needed, Eq. 1 reduces to a 2D convolution product (Keck et al., 2013b), denoted $**$ in the following. This is possible in the DWM framework since $U_{MF,dwm}$ is considered to be steady and thus the elements of the wake centre time series can be permuted without affecting the results of Eq. 1. It gives:

$$\overline{U_{FF,dwm}}(y,z) = U_{MF,dwm}(y,z) ** f_c(y,z) = \int\int U_{MF,dwm}(y-y_c, z-z_c) f_c(y_c,z_c) dy_c dz_c \quad (2)$$

where $f_c(y,z)$ is the probability density function (PDF) of the wake centre position, normalised such as $\int\int f_c(y_c,z_c)dy_c dz_c = 1$. Here and in the following, the Reynolds decomposition is used to write any unsteady field $X(t)$ as a sum of a mean and a fluctuating part: $X(t) = \overline{X} + X'(t)$.

In the DWM, the total turbulence (defined as the temporal variance of the velocity field) in the FFOR in the wake can be computed as the sum of two components:

$$k_{FF,dwm}(x,y,z) = k_{a,dwm}(x,y,z) + k_{m,dwm}(x,y,z) \quad (3)$$

where k_a is the rotor-added turbulence, mainly driven by the shear generated by the velocity deficit in the wake and k_m is the meandering turbulence, generated by the lateral and vertical displacements of the wake. Similarly to Eq. 2, these two components can be written (Keck et al., 2013b):

$$k_{a,dwm}(y,z) = \int\int k_{MF,dwm}(y-y_c, z-z_c) f_c(y_c,z_c) dy_c dz_c = k_{MF,dwm}(y,z) ** f_c(y,z) \quad (4)$$

$$k_{m,dwm}(y,z) = \int\int \left(U_{MF,dwm}(y-y_c, z-z_c) - \overline{U_{FF,dwm}}(y,z)\right)^2 f_c(y_c,z_c) dy_c dz_c \quad (5)$$

$$= U^2_{MF,dwm}(y,z) ** f_c(y,z) - \overline{U_{FF,dwm}}^2(y,z) \quad (6)$$

where $k_{MF,dwm}$ is the modelled turbulence in the MFOR, i.e. the turbulence that would be measured if there was no meandering. In the DWM model, an empirical scaling of $U_{MF}(y,z)$ with a factor $k_{mt}(y,z)$ is used to compute $k_{MF,dwm}$ (Madsen et al., 2010; Conti et al., 2021). Equation 6 is obtained by developing Eq. 5 and simplifying with Eq. 2. The added value of such approach is that it allows writing the velocity and the turbulence in the FFOR as a function of the same fields in

https://doi.org/10.5194/wes-2022-46
Preprint. Discussion started: 31 May 2022

the MFOR, where they are presumed to be only dependent to the turbine's operating conditions, thus less complex and easier to model.

The objective of this work is to write the velocity and turbulence in the FFOR as a function of the velocity and turbulence in the MFOR and show the underlying DWM assumptions that neglect some terms. The importance of these missing terms for both velocity and turbulence is evaluated. The reference results come from large eddy simulations (LESs) of an isolated wind turbine wake over a flat terrain. Three cases of stability, approximately corresponding to the SWiFT benchmark (Doubrawa et al., 2020), are simulated using Meso-NH (Lac et al., 2018) with an actuator line method (ALM) (Joulin et al., 2020; Jézéquel et al., 2021).

This work is separated into two papers. In the present one, the breakdown of the velocity and turbulence is presented and applied to the LESs datasets. In the companion paper, the results are used to build a new analytical model for velocity and turbulence in the wake of a wind turbine. The first part of the present work is dedicated to the development of the velocity and turbulence breakdowns, i.e. the expression of the velocity and turbulence fields in the FFOR as a function of their counterparts in the MFOR. In the second part, the numerical framework is detailed: it describes the SWiFT cases, the LES code Meso-NH, the numerical setup, the wake tracking algorithm and the limitations of these tools. In the third part, the neutral LES dataset is used to quantify the error induced by the approximations necessary to write Eqs. 2 and 3. In the fourth part, the dependence of k_a and k_m on the atmospheric stability is studied and the shape of all the terms in the turbulence breakdown equation is described.

2 Analytical development

To lighten the mathematical formulations, the notation $\widehat{a(y,z)} = a(y - y_c(t), z - z_c(t))$ will be used to express the switch between FFOR and MFOR (i.e. Eq. 1). This operation can be interpreted as an unsteady translation of the field a by the meandering: the stronger the meandering, the more spread will be $\widehat{a}$. It is important to note that a can be steady or unsteady, but $\widehat{a}$ is always unsteady. For any variables a and b, the following properties hold:

$$\widehat{a} + \widehat{b} = \widehat{a+b}. \tag{7}$$

$$\widehat{a} \cdot \widehat{b} = \widehat{a \cdot b}. \tag{8}$$

$$\widehat{\overline{a}} \neq \overline{\widehat{a}}. \tag{9}$$

$$\overline{\widehat{\overline{a}}} = \overline{a} ** f_c. \tag{10}$$

Properties 7 and 8 are obtained from the linearity of the translation opertor. Property 9 is trivial since $\widehat{\overline{a}}$ is time-dependant and $\overline{\widehat{a}}$ is not. Property 10 can be demonstrated by defining f_c as a sum of indicator functions and applying a Taylor development. Using the $\widehat{.}$ notation and applying the Reynolds decomposition to U_{MF} allows to re-write Eq. 1 as:

$$U_{FF} = \widehat{U_{MF}} = \widehat{\overline{U_{MF}}} + \widehat{U'_{MF}} \tag{11}$$

https://doi.org/10.5194/wes-2022-46
Preprint. Discussion started: 31 May 2022

eawe european academy of wind energy
Open Access WIND ENERGY SCIENCE DISCUSSIONS

The mean velocity in the FFOR can directly be deduced by applying the averaging operator to this equation:

$$\overline{U_{FF}} = \underbrace{\overline{\widehat{\overline{U_{MF}}}}}_{(I)} + \underbrace{\overline{\widehat{U'_{MF}}}}_{(II)} \tag{12}$$

From Eq. 10, it appears that the term (I) is the convolution of $\overline{U_{MF}}$ with f_c, and can be viewed as a pure mean velocity term: it is null only if the mean velocity is null. Conversely, the term (II) is here viewed as a cross-term because it can be equal to 0 either if there is no meandering ($\widehat{x} = x$) or if there is no turbulence in the MFOR ($U'_{MF} = 0$). In the DWM model, $U_{MF,dwm}$ is steady so $U_{MF,dwm} = \overline{U_{MF,dwm}}$ and $U'_{MF,dwm} = 0$, thus Eqs. 2 and 12 are equivalent. The assumption of steady flow in the MFOR for analytical or DWM models is equivalent to the assumption that term (II) of Eq. 12 is negligible. Since $U'_{MF} = 0$ is not necessarily true in real cases (nor in LESs, which are used here) this hypothesis must be verified, which is one of the objectives of the present work.

For the turbulence equation, one can write from Eqs. 11 and 12:

$$\overline{U^2_{FF}} = \overline{\widehat{\overline{U_{MF}}}^{\,2}} + 2\overline{\widehat{\overline{U_{MF}}}\widehat{U'_{MF}}} + \overline{\widehat{U'_{MF}}^{\,2}} \tag{13}$$

$$\overline{U_{FF}}^2 = \overline{\widehat{\overline{U_{MF}}}}^2 + 2\overline{\widehat{\overline{U_{MF}}}}\,\overline{\widehat{U'_{MF}}} + \overline{\widehat{U'_{MF}}}^2 \tag{14}$$

The total turbulence in the FFOR can then be written as a function of the preceding quantities:

$$\begin{aligned} k_{FF} &= \overline{U'^2_{FF}} = \overline{U^2_{FF}} - \overline{U_{FF}}^2 \\ &= \overline{\widehat{\overline{U_{MF}}}^{\,2}} - \overline{\widehat{\overline{U_{MF}}}}^2 + 2\left(\overline{\widehat{\overline{U_{MF}}}\widehat{U'_{MF}}} - \overline{\widehat{\overline{U_{MF}}}}\,\overline{\widehat{U'_{MF}}}\right) + \overline{\widehat{U'_{MF}}^{\,2}} - \overline{\widehat{U'_{MF}}}^2 \\ &= \underbrace{\overline{\widehat{\overline{U_{MF}}}^{\,2}} - \overline{\widehat{\overline{U_{MF}}}}^2}_{(III)} + \underbrace{2\mathrm{cov}\left(\widehat{\overline{U_{MF}}}, \widehat{U'_{MF}}\right)}_{(V)} + \underbrace{\overline{\widehat{\overline{U'^2_{MF}}}}}_{(IV)} + \underbrace{\overline{\widehat{(U'^2_{MF})'}}}_{(VI)} \underbrace{- \overline{\widehat{U'_{MF}}}^2}_{(VII)} \\ &= \underbrace{k_m}_{(III)} + \underbrace{k_a}_{(IV)} + \underbrace{2\mathrm{cov}\left(\widehat{\overline{U_{MF}}}, \widehat{U'_{MF}}\right)}_{(V)} + \underbrace{\overline{\widehat{(U'^2_{MF})'}}}_{(VI)} \underbrace{- \overline{\widehat{U'_{MF}}}^2}_{(VII)} \end{aligned} \tag{15}$$

The term (III), also written k_m in the following, is the turbulence purely induced by meandering: in the case of a meandering steady wake i.e. $U'_{MF} = 0$, Eq. 15 reduces to this term only. In the DWM model, the wake in the MFOR is steady, but a rotor added turbulence term is added to model the small-scale turbulence that exists in the MFOR in real cases. This rotor added turbulence can be calibrated from the MFOR turbulence in reference data i.e. term (IV) of Eq. 15. It is the turbulence purely induced by the rotor: in absence of meandering ($\widehat{x} = x$), the equation reduces to this term only, also written k_a in the following.

Through Eq. 3, it is assumed in the DWM that the wake turbulence is separated between two terms: one purely induced by the meandering ($k_{m,dwm}$, related to term (III)) and the other purely induced by the rotor ($k_{a,dwm}$, related to term (IV)). The

https://doi.org/10.5194/wes-2022-46
Preprint. Discussion started: 31 May 2022

analysis presented above shows that three cross-terms are neglected under this assumption. Term (V) is the covariance of $\overline{\widehat{U_{MF}}}$ and $\widehat{U'_{MF}}$, term (VI) is the remaining of $\overline{\widehat{U'_{MF}}^2}$ when subtracting the rotor-added turbulence in the FFOR $k_a = \overline{\widehat{U'^2_{MF}}}$ (it can be viewed as the varying part of the MFOR turbulence) and term (VII) is the square of the term (II). It is a pure dissipation term as it is always negative. Like the term (II), these are cross-terms since they are equal to zero if either the turbulence in the MFOR or the meandering is null.

Similarly to the velocity field, Eq. 15 shows that when calibrating a DWM-type model against realistic data (measurement or high-fidelity simulation, denoted $._{cal}$), if it is assumed that $U_{MF,dwm} = \overline{U_{MF,cal}}$ and $k_{MF,dwm} = \overline{U'^2_{MF,cal}}$, then there will be three missing terms: (V), (VI) and (VII). Like term (II) for the velocity, these terms cannot be computed directly from a steady model of the velocity in the DWM so similarly to term (IV), they must be modelled differently. In other words, in the DWM formulation (Eq. 3), terms (III) and (IV) are retained and terms (V), (VI) and (VII) are neglected.

3 Methodology

3.1 The SWiFT benchmark

The breakdowns of the mean velocity and turbulence fields in the FFOR described in Sect. 2 is applied to three LESs cases. These datasets are the result of simulations that reproduce the SWiFT benchmark (Doubrawa et al., 2020) with the LES code Meso-NH (Lac et al., 2018). The simulated turbine is a modified version of the Vestas V27: it is a three-bladed rotor with a diameter of $D = 27$ m and a hub height of 32.1 m. The orography of the terrain is neglected, and three cases of stability are simulated: near-neutral, unstable and strongly stable. The simulations are classified with the Monin-Obukhov length:

$$L_{MO} = -\frac{u_*^3 \theta}{\kappa g \overline{\theta' w'}} \tag{16}$$

where $u_* = (\overline{u'w'}^2 + \overline{v'w'}^2)^{1/4}$ is the friction velocity, $\overline{\theta' w'}$ is the turbulent potential temperature flux, and θ is the potential temperature. All these variables are computed at $z = 10$ m above the ground. κ and g are the Von Kármán and earth gravity constants. For the neutral, unstable and stable cases, the stability parameters at $z = 10$ m are respectively $z/L_{MO} = \{0.003, -0.16, 0.60\}$, the inflow velocities at hub height are $U_h = \{8.4, 6.2, 3.7\}$ m s^{-1}, the inflow streamwise turbulence intensities at hub height are $TI_x = \{11.2, 12.3, 4.7\}$ % and the thrust coefficients are $C_T = \{0.79, 0.81, 0.82\}$.

3.2 The Meso-NH LES solver

Meso-NH (MESOscale Non Hydrostatic) is a finite volume, open-source research code for ABL simulations developed by the Centre National de Recherches Météorologiques and the Laboratoire d'Aérologie. The model is described in detail in Lafore et al. (1998); Lac et al. (2018). The filtered Navier-Stokes and energy conservation equations are resolved on an Arakawa C-grid. The unknowns of the system are the velocities (U_x, U_y and U_z) and the potential temperature θ. A constant density profile $\rho(z)$ is imposed, except for the buoyancy term (anelastic assumption) and the vertical velocity is driven by the vertical

https://doi.org/10.5194/wes-2022-46
Preprint. Discussion started: 31 May 2022

pressure gradient and the gravity (non-hydrostatic set of equations). The Coriolis force is added to the momentum equation, as well as a large-scale forcing term, which is imposed by the user through a 2-D geostrophic wind U_g.

The turbulence closure is of order 1.5: an additional equation is introduced for the subgrid kinetic energy e_{sgs} and the other subgrid terms are modelled as functions of the resolved quantities, e_{sgs} and a mixing length L_m (Cuxart et al., 2000). The mixing length is related to the grid size and stratification through the Deardorff formulation (Deardorff, 1980). This set of equations is discretised spatially with a fourth-order centred scheme and temporally with a fourth-order Runge-Kutta scheme.

To model the wind turbine, the ALM is used, following Sørensen and Shen (2002). This method has been implemented in Meso-NH, validated against the NewMexico wind tunnel experiments (Joulin et al., 2020) and against the *in situ* measurements and LESs codes of the SWiFT benchmark (Jézéquel et al., 2021). A grid nesting technique allows to couple two or more computational domains of different sizes, temporal and spatial resolutions (Stein et al., 2000). The velocity field of a father domain D_i is interpolated to the boundaries of a son domain D_{i+1}. Hence, the resolution can be brought below the metre (necessary here to have 30 mesh points per blade as recommended in Troldborg (2009)), while still taking into account the large-scale behaviour of the ABL.

3.3 Numerical parameters

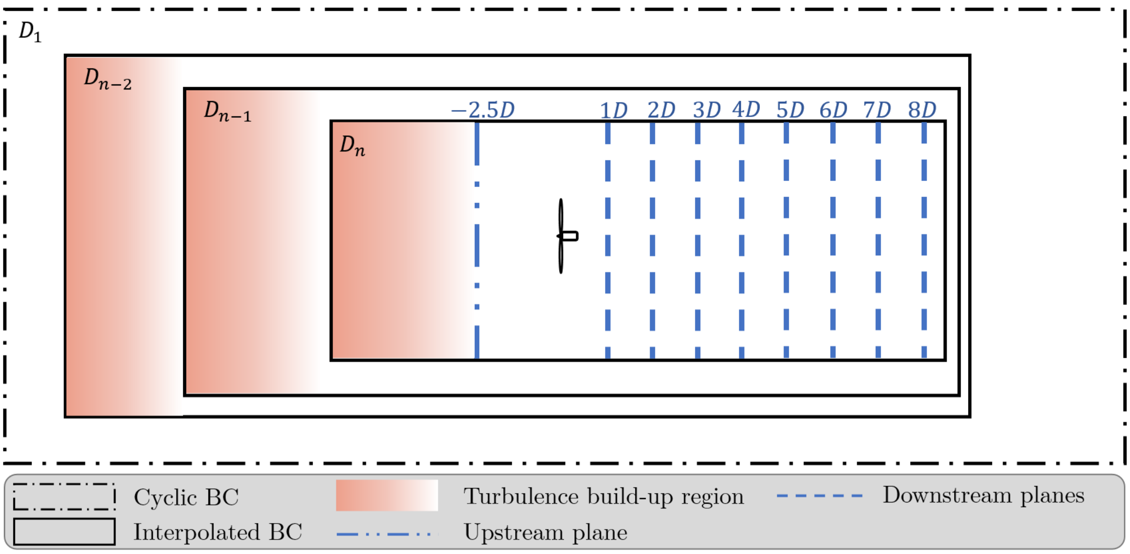

Figure 2. Schematic of the simulation set-up with Meso-NH.

The numerical parameters used for the three simulations are presented in Table 1 for the different domains of the grid nesting. The size of the horizontal mesh depends on the domain D_i but in Meso-NH the vertical mesh is the same for every domain. In the induction and the wake regions, the vertical discretisation ΔZ is set to have isotropic cells in the most refined domain i.e. D_4 in the neutral and unstable cases and D_2 in the stable case. The bottom boundary condition is determined by the subgrid

https://doi.org/10.5194/wes-2022-46
Preprint. Discussion started: 31 May 2022

heat $\overline{w'\theta'}$ and momentum $\overline{w'u'}$ fluxes. The heat flux is prescribed and governs the evolution of θ in the middle of the first cell, along with other resolved processes such as advection. The momentum flux at the surface is computed according to the Monin-Obukhov similarity laws, depending on the roughness length, wind at the middle of the first grid mesh and heat flux. It is used to compute the velocity at the first grid mesh.

	Neutral				Unstable				Stable	
	D_1	D_2	D_3	D_4	D_1	D_2	D_3	D_4	D_1	D_2
z_0 [mm]	14				14				14	
$\overline{w'\theta'}$ [K m s^{-1}]	–0.0020				0.0247				-0.0047	
ABL height [m]	1000				1000				200	
U_g [m s^{-1}]	(u=11.42, v=-3.7)				(u=8.1, v=-1.2)				(u=7.6, v=-3.1)	
ΔZ [m]	0.5				0.5				0.4	
$\Delta X = \Delta Y$ [m]	20	4	1	0.5	20	4	1	0.5	1.2	0.4
L_X [m]	6000	3200	640	432	12000	4000	1080	500	540	480
L_Y [m]	2400	1600	320	216	6000	2000	540	250	300	180
Δt [ms]	200	100	50	8	100	100	50	10	140	11
Simulation time [s]	4800				2400				60	
Ω [rad s^{-1}]	4.56				3.89				2.79	
γ [deg]	–0.75				–0.75				–0.75	

Table 1. Numerical parameters used in Meso-NH.

The flowfield is initialised with a constant-velocity profile equal to the geostrophic wind. A constant-temperature profile is set up to an arbitrary defined ABL height, capped by an inversion region of intensity of 5 K over a depth of 50 m. The geostrophic wind, ABL height, surface roughness z_0 and kinematic vertical heat flux are chosen to be as close as possible to the SWiFT measurements in terms of velocity, wind direction, TKE and stability parameter.

In the first domain D_1, the boundary conditions are cyclic in order to let the turbulence establish, with dimensions L_X and L_Y larger than the largest eddies of the flow. In a stable ABL, these eddies are smaller, which is why a smaller domain D_1 is suited, and inversely for the unstable case. After an initialisation of turbulence in domain D_1, the nested domains (D_2, D_3 and D_4) are successively created. In each nested domain D_i, a region in which the turbulent flow adapts to the finer resolution (in brown in Fig. 2) appears near the inflow. The next domain D_{i+1} must avoid it, so a spectral analysis (not shown here) has been carried out to measure the end of this perturbed region. The time step in every domain is driven by the CFL condition, except for the finest domain, where it is equal to the time needed for the tip of the blades to cross one cell.

The ALM is activated once the flow is established in the most refined domain, and after a 10 minutes spin-up to let the wake flow establish, the instantaneous velocity is extracted at one plane upwind of the turbine and several planes downwind, according to Fig. 2. Note that the simulation time is case-dependent: 80, 40 and 10 minutes for the neutral, unstable and stable cases.

https://doi.org/10.5194/wes-2022-46
Preprint. Discussion started: 31 May 2022

The rotational velocity of the wind turbine Ω and pitch of the blades γ are set constant to a value interpolated in the controller table of the turbine with the upstream velocity at hub height U_h, and a simple implementation of the nacelle and the tower is used (corresponding to Stevens et al. (2018)).

3.4 Wake tracking

The wake meandering is characterised by the time series of the wake centre coordinates $y_c(x,t)$ and $z_c(x,t)$. Even though it is a very handy concept from a theoretical point of view, defining the centre of the wake or even its borders is difficult, especially when the wake is developing inside a turbulent boundary layer. Indeed, the turbulent structures can move, twist or even split the wake, and low-velocity eddies can be mistaken for the wake.

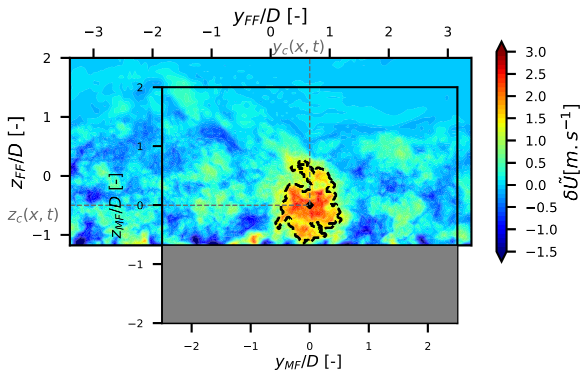

Figure 3. Result of the wake tracking at an arbitrary time step at x=6D downstream. The detected isocontour is in dashed line and the detected wake centre is represented by a diamond.

To determine the wake centre at each time step, an algorithm based on the conservation of momentum in the wake is used (Quon et al., 2020). First, the 2D velocity and momentum deficits are computed at each time step and for each downstream plane:

$$\delta\tilde{U} = \tilde{U}_{ref}(x,y,z,t) - \tilde{U}(x,y,z,t) \tag{17}$$

$$\delta\tilde{M} = \tilde{U}(x,y,z,t)\left[\tilde{U}_{ref}(x,y,z,t) - \tilde{U}(x,y,z,t)\right] \tag{18}$$

where U is the streamwise velocity in the simulation and U_{ref} is the streamwise velocity in a reference simulation i.e. a simulation without wind turbine but with the same inflow and boundary conditions. This operation allows removing the atmospheric shear and low-velocity eddies of the ABL that can be mistaken with the wake. A moving-average operator $\tilde{.}$ is applied on the velocity field with a window of seven frames (i.e. seven seconds). This window size is chosen to smooth the data and facilitate the wake tracking while not impacting significantly the resulting time series of the wake centre's coordinates. The wake outline is then defined as the best fit of $\delta\tilde{U}$ isoline that encloses a surface S such as:

https://doi.org/10.5194/wes-2022-46
Preprint. Discussion started: 31 May 2022

$$\rho \int\int_S \delta \tilde{M} dS = \overline{T} \quad (19)$$

where ρ is the density of the fluid and $\overline{T}$ is the mean thrust. The wake centre is then computed as the velocity deficit centroid of S. An illustration of this algorithm at $x/D = 6$ for an arbitrary time step is given in Fig. 3. This post-processing is performed with the python post-processing tool SAMWICH (Quon et al., 2020) where this algorithm is referenced as *Constant Flux* or *CstFlux*. This algorithm has been chosen for its high success rate and physically-consistent fields in the MFOR. Finally, several extreme values of y_c and z_c are considered outliers (in the worst case it concerns about 5% of the frames) and manually removed from both the FFOR and MFOR datasets.

3.5 Limitations

In order to compute terms (I) to (VII) of Eqs. 12 and 15, it is needed to start from the unsteady field U_{MF} and apply the Reynolds decomposition and operator $\widehat{\cdot}$ i.e. reverse Eq. 1. To avoid losing any data, one should compute the MFOR on a grid spanning from $y_{min,FF} + \min(y_c)$ to $y_{max,FF} + \max(y_c)$ and similarly in the vertical direction. For strong meandering cases, it would result in a very large grid that would be computationally costly to manipulate. It has thus been decided to restrain the MFOR to $\{y,z\} = \{[-2.5D, +2.5D], [-2D, 2D]\}$. Consequently, some data is missing in the MFOR, leading to unavoidable small differences between the left and right hand-sides of Eqs. 12 and 15.

Given that the ground is located around $z_{FF} \approx -1.2D$, the velocity field at $U_{MF}(z_{MF} < -1.2D - z_c(t))$ is undefined since it is located under the ground (the grey region in Fig. 3) so this part of the velocity field is ignored when computing the mean velocity and TKE in the MFOR. Consequently, the statistics (mean and variance) near the ground in the MFOR are computed with fewer samples than those at higher positions.

The wake tracking and the computation of each term of Eqs. 12 and 15 is a costly post-processing, in terms of computational resources and memory. Given the relatively low time step imposed by the ALM it was not feasible to apply this algorithm to every LES time step, so a sampling frequency of 1 Hz has been chosen to store the output velocity field of Meso-NH. This means that all the variations of the wind velocity at frequencies higher than 1 Hz are not taken into account in this work, nor is the subgrid turbulence. The latter is negligible in the unstable and neutral cases but can reach more than 10% in the stable case.

Finally, only the streamwise component of the velocity is computed in the following, in both MFOR and FFOR. In all the following, the mean streamwise component of the velocity will be noted U_x, and the streamwise turbulence $k_x = \overline{u'u'}$ will be used to differentiate from the total TKE.

4 Error induced by neglecting the cross-terms.

Once the Meso-NH simulations are performed, U_x and k_x in the FFOR are directly computed as the mean and variance of the unsteady streamwise velocity field. The wake tracking algorithm described in Sect. 3.4 is applied to get the unsteady

https://doi.org/10.5194/wes-2022-46
Preprint. Discussion started: 31 May 2022

streamwise velocity field in the MFOR. The Reynolds decomposition and meandering operator $\widehat{\cdot}$ can then be applied to get the values of terms (I) and (II) of Eq. 12 and terms (III), (IV), (V), (VI) and (VII) of Eq. 15.

The objective of this section is to quantify the importance of each term and to estimate the error induced by neglecting the cross-terms in the velocity and turbulence breakdowns, for instance in the DWM model or in the model developed in the
240 companion paper. The focus is on the neutral case but similar conclusions can be drawn from the other stability cases. The normalised root-mean-square error (RMSE) indicator (Eq. 20) is used to quantify different levels of approximation with the actual results in the FFOR.

$$\mathrm{RMSE} = \sqrt{\frac{\sum_{i=1}^{N}(\alpha-\alpha_p)^2}{N}}/(\alpha_{max}-\alpha_{min}) \tag{20}$$

where α is the reference value (directly extracted from Meso-NH), α_p is the predicted value, N is the number of samples
245 and $\alpha_{max}-\alpha_{min}$ is the range of α over those samples. When the RMSE is computed on a $Y-Z$ plane, only the truncated plane ($y \in [-2D, 2D], z \in [-1D, 1D]$) is used to avoid edge effects and then N denotes the number of mesh points in this plane.

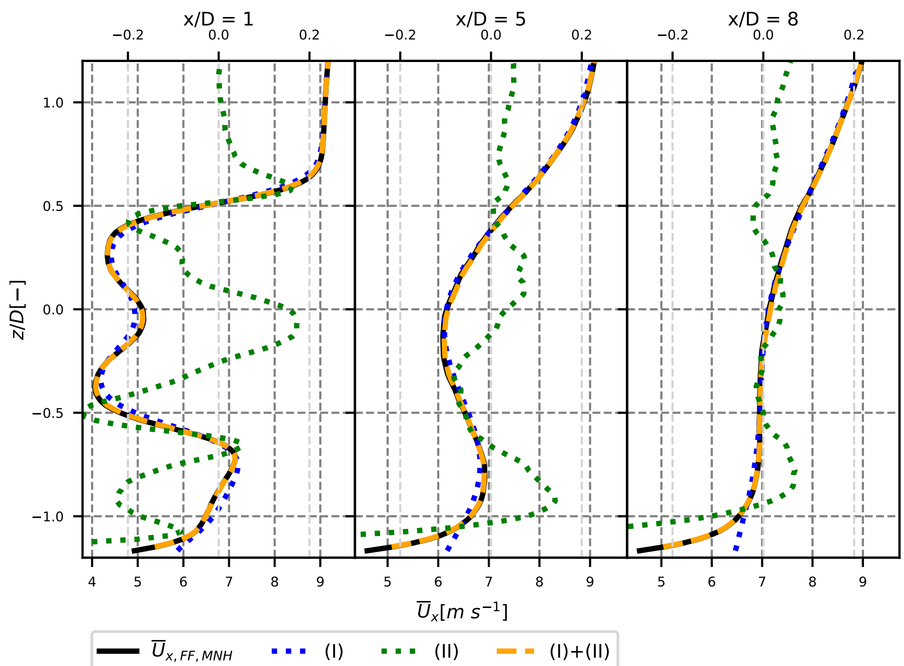

Figure 4. Contribution of terms (I) and (II) from Eq. 12 to the velocity in the wake of the neutral case, compared to the velocity in the FFOR. Term (II) is plotted on a different scale (top axis).

https://doi.org/10.5194/wes-2022-46
Preprint. Discussion started: 31 May 2022

4.1 Velocity field

In Eq. 12, the velocity is separated into two terms, (I) and (II). The vertical profiles of these terms are plotted in Fig. 4 for several downstream positions. The term (I), which is the convolution of the velocity in the MFOR with the distribution of wake centre position, actually fits very well with the velocity in the FFOR. Small differences only appear in the near wake. Term (II) is plotted on a secondary axis (displayed at the top of the figure) to show that it has a negligible value: less than 0.3 m/s in absolute value, i.e. less than 4 %. In the stable case it is even more negligible but in the unstable case (both are not shown here), it takes slightly larger values of about 0.5 m s^{-1} i.e. 10 % at the wake centerline in the near wake. As it can be seen at the bottom of the profiles, the main role of this term in the far wake is to reproduce the shear near the ground that is missing in the MFOR, and thus not present in term (I).

From this first observation, it seems acceptable to neglect the term (II). The effect of this assumption can also be measured with a global variable. It has been chosen to investigate the error induced by neglecting the term (II) on the available power, since predicting the power output of a farm is a direct application of analytical models. The available power is here defined as:

$$P_a(x) = \int_S \rho \overline{U}_x^3(x,y,z)dydz \tag{21}$$

where S is the surface of a virtual wind turbine located at position x behind the wake-emitting turbine, with hub height at the same lateral and vertical position: $y = 0$ and $z = 0$ position. This quantity is computed for (I) and (I)+(II) at each available position downstream of the wind turbine, and compared to the same quantity directly computed on the Meso-NH field in the FFOR $P_{a,FF}$.

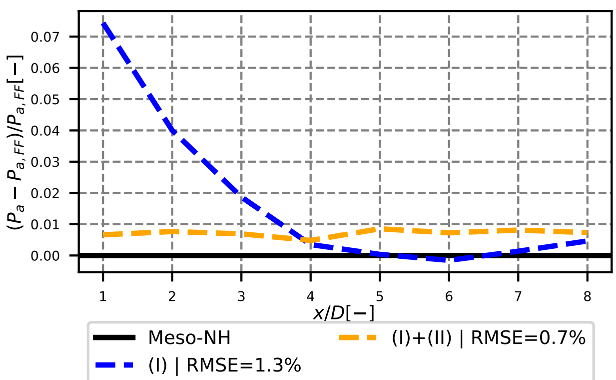

Figure 5. Available power predicted by (I) (blue) and (I)+(II) (yellow), normalised with the results in the FFOR (black line).

From Fig. 5, it appears that neglecting term (II) leads to a slight overestimation of the available power in the near wake of the wind turbine. The estimation is however fairly good, especially for a wind turbine located further than 3D downstream where the overestimation drops below 2 %. The relative error is larger in the unstable case (reaching about 6 % at 8D downstream), and much lower in the stable case (less than 0.3 %). If the velocity near the ground is not of interest, approximating the FFOR

https://doi.org/10.5194/wes-2022-46
Preprint. Discussion started: 31 May 2022

velocity as the term (I) alone as it is done in the DWM can thus be acceptable given the low error on estimated power. This is especially relevant since the term (II) seems very chaotic (see Fig. 4) and thus hard to model.

4.2 Turbulence field

The same study is performed for the turbulence field in the wind turbine wake. The vertical turbulence profiles are plotted for different levels of approximation, at different positions downstream in Fig. 6. In the DWM model, only the meandering (III) and rotor-added turbulence (IV) terms are retained. This corresponds to the blue curve: despite an overall good order of magnitude, it can be seen that the vertical asymmetry is not sufficiently pronounced, leading to an underestimated value of k_x at the top tip and overestimated value at the bottom tip. This issue, especially true in the near wake, has already been observed in another work that used an equation similar to Eq. 15 (Conti et al., 2021) to compare the DWM results to *in situ* measurements. If horizontal profiles at hub height are plotted instead (shown in the companion paper), the results are much better and the DWM approximation seems suitable, for the neutral but also the unstable and stable cases.

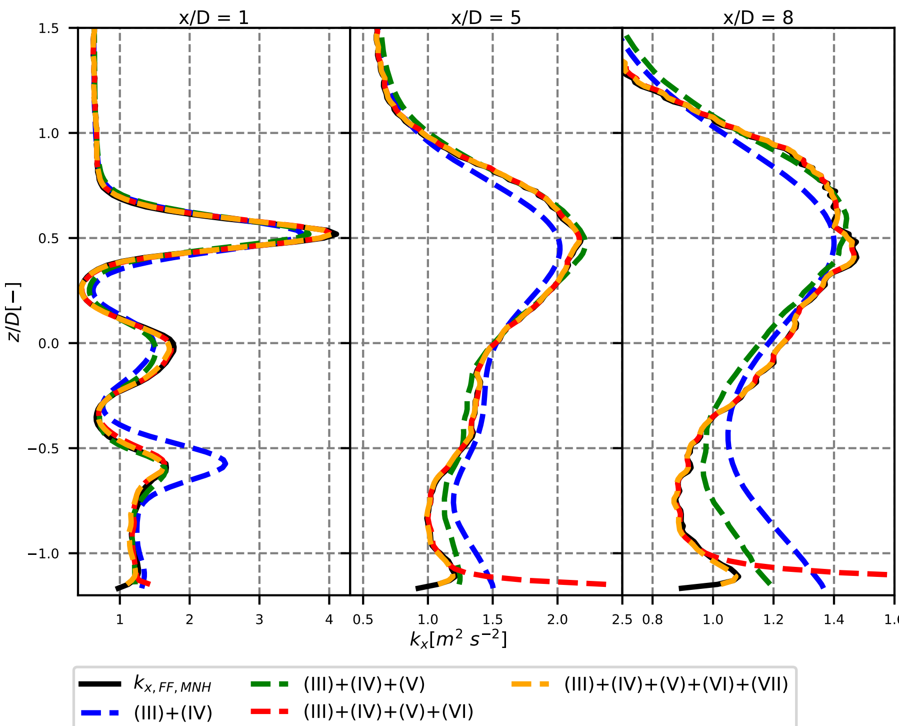

Figure 6. Velocity in the wake of the wind turbine for different levels of approximation.

Adding the covariance term (V) along with terms (III) and (IV) (green curve in Fig. 6) corrects for most of the vertical asymmetry of the turbulence profiles and leads to a rather good estimation of the maximum turbulence values at the top and bottom tips. The main effect of adding term (VI) (red curve) is to take the spatial small-scale variations into account, bringing the total k_x even closer to its reference value. As pointed out previously, the term (VII) is the square of the term (II): like the latter, it mainly has an effect near the ground but is otherwise negligible.

In order to quantify more clearly these differences, the maximum axial turbulence $k_x^M(x)$ is studied. It is computed directly in the FFOR ($k_{x,LES}^M(x)$) and for different levels of approximation from Eq. 15. Their evolution with the downstream distance is plotted in Fig. 7, normalised by $k_{x,LES}^M(x)$ and the same colour convention as in Fig. 6 is used.

Neglecting the cross-terms leads to an underestimation of about 6 % to 12 % of the maximum turbulence in the wake. Adding the covariance term (V) allows to bring this number down between 2 % and 6 %, and adding term (VI) to this total leads to a negligible underestimation (around 1 %). Term (VII) has a negligible effect on the maximum turbulence (orange and red curves are superimposed). The remaining gap is attributed to the error reconstruction due to a MFOR not being large enough (see Sect. 3.5).

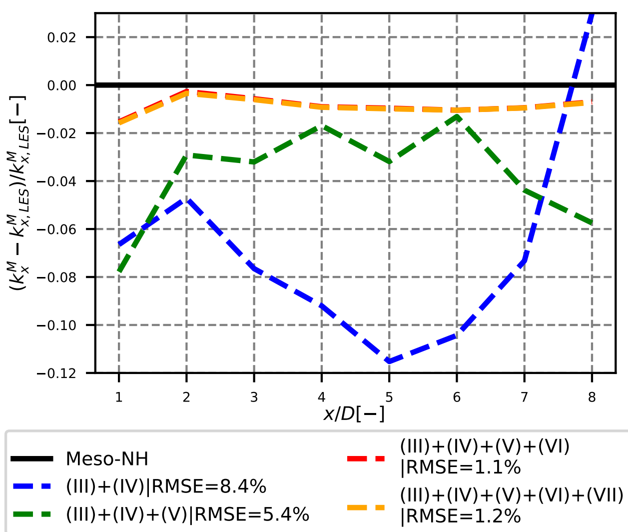

Figure 7. Normalised maximum turbulence in the wake for different levels of approximation. The RMSE of k_x^M averaged over all the x positions is displayed.

For the two other cases of stability, the same orders of magnitude are observed for the different k_x approximations: adding the convolution term (V) reduces the relative underestimation of k_x^M by at least half and using (III)+(IV)+(V)+(VI) leads to a fairly good approximation. Term (VII) is almost negligible in every case. It is important to note that in the simulations, the maximum k_x is observed near the top tip of the blade except in the unstable case where it gradually moves towards the wake centre.

It has been shown in this section that neglecting term (II) in the DWM model leads to a rather accurate velocity deficit in the wake and a reasonable estimation of the available power (less than 2% overestimation) for a wind turbine inside the wake, as long as it is positioned beyond $x/D = 3$. For the turbulence breakdown, the term (VII) is also negligible, but the vertical turbulence profiles are prone to errors when terms (V) and (VI) are not taken into account, leading to an underestimation of

https://doi.org/10.5194/wes-2022-46
Preprint. Discussion started: 31 May 2022

the maximum turbulence in the wake. It is now needed to compare the shapes and the relative magnitude of these terms before modelling them.

5 Analysis and interpretation of the turbulence breakdown

In this section, the turbulence fields in the wake of the wind turbine are compared for the three cases of stability. The influence of atmospheric stability on each term of Eq. 15 is highlighted and the shape of these terms in the Y-Z plane is analysed.

5.1 Shape and values of the terms

The values of each term of Eq. 15 at different Y-Z planes downstream of the turbine in the FFOR are displayed in Figs. 8, 9 and 10 for the neutral, unstable and stable cases respectively. The terms are normalised by the maximum total turbulence in the FFOR $k^M_{x,LES}(x)$ in the 2D plane, so the scale is approximately the fraction of the total axial turbulence represented by each term. Term (IV) contains both the rotor-added turbulence and the inflow turbulence, which is removed by subtracting the reference turbulence field in the MFOR $k_{x,ref,MF} = \overline{U'^2_{x,ref,MF}}(x,y,z)$ taken from the reference simulation (the same simulation without the turbine, see Sect. 3.4) at the same location than the waked turbulence field. In the MFOR the rotor added axial turbulence is thus defined as the difference of axial turbulence between the simulation with and without the wind turbine:

$$\Delta k_{x,MF}(x,y,z) = \overline{U'^2_{x,MF}}(x,y,z) - \overline{U'^2_{x,ref,MF}}(x,y,z) \tag{22}$$

Note that the $y_c(t)$ and $z_c(t)$ computed in the simulation with a turbine are re-used to compute the reference MFOR field and to apply operator $\widehat{\cdot}$ to the reference data. The rotor added turbulence can then be defined in the FFOR as:

$$\Delta(\text{IV}) = \overline{\widehat{\overline{U'^2_{MF}}}} - \overline{\widehat{\overline{U'^2_{ref,MF}}}} = (\text{IV}) - \overline{\widehat{k_{x,ref,MF}}} \tag{23}$$

The reference turbulence in the FFOR $\overline{\widehat{k_{x,ref,MF}}}$ is also plotted in the last line of Figs. 8, 9 and 10 to quantify how the wake turbulence is going back its unperturbed value: the closest $\overline{\widehat{k_{x,ref,MF}}}$ is to 1, the most dissipated is the wake.

For the neutral case of stability (Fig. 8), the meandering (III) and rotor-added Δ(IV) terms have similar orders of magnitude and contain most of the total wake added turbulence. However, the covariance term (V) cannot be ignored as it rebalances the total turbulence of about $\pm 10\%$ between the top and bottom regions of the wake, as it has been seen in Fig. 6. Term (VI) also shows non-negligible values, in particular in the far wake where it progressively takes values closer to the other terms, but the shape of this term seems to be randomly distributed (contrarily to term (V) which is located in the rotor-swept area). As stated in Sect. 4, the term (VII) is negligible, except near the ground.

Figure 9 has been plotted similarly to Fig. 8 with the results of the unstable case. The meandering term (III) is dominant over the others and the wake is quickly dissipating. The rotor-added turbulence has lower relative values and is more spread than

https://doi.org/10.5194/wes-2022-46
Preprint. Discussion started: 31 May 2022

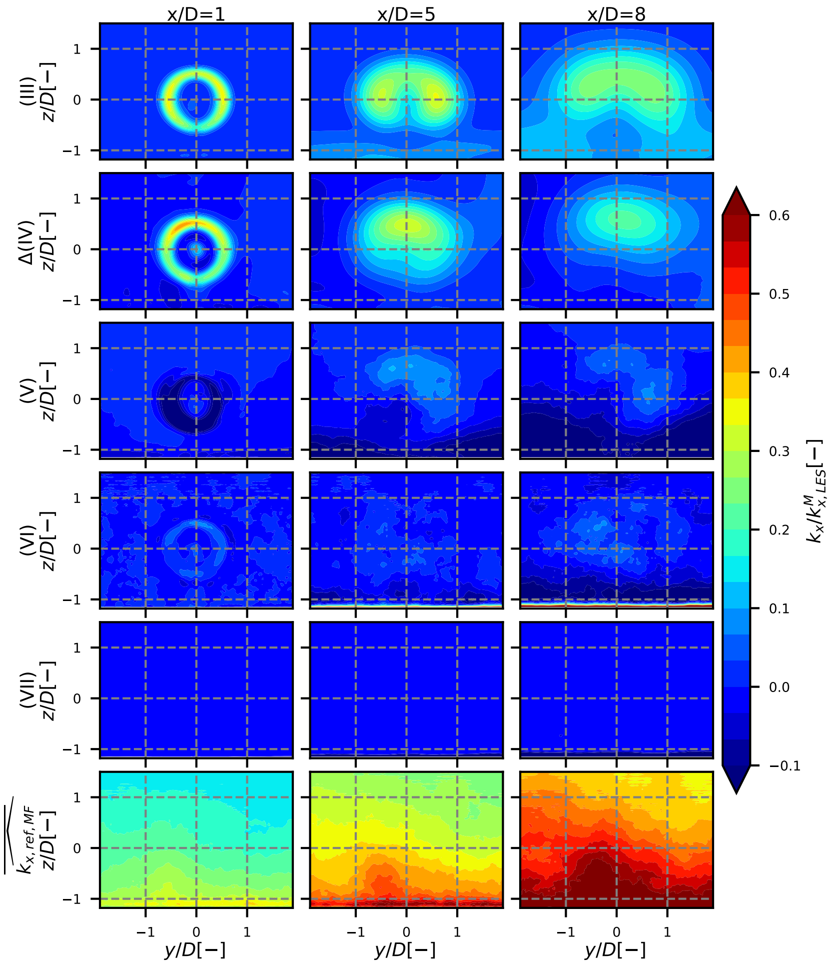

Figure 8. 2D maps of the different terms in Eq. 15 for the neutral case. The different lines stand for the different terms and each column is a different position downstream. The values are scaled by the maximum TKE in the FFOR at the given x position.

in the neutral case. This is due to larger meandering in the unstable case i.e. a PDF f_c with larger values at the edge and thus more spreading caused by the operator $\widehat{\cdot}$. The covariance term is also not negligible: here it takes values between terms Δ(IV) and (III) in the far wake. In this case, the term (V) is symmetric about the vertical axis instead of the horizontal one. Term (VI) shows lower values, that seem to be randomly distributed as in the neutral case. Term (VII) is still negligible.

In the stable case (Fig. 10), it is the rotor-added turbulence that is largely predominant over the meandering and even the upstream terms. This can be explained by the fact that meandering is very weak, so the term (III) is low, the term (IV) is almost not spread by the convolution with f_c, and the wake is barely dissipated, even at $x/D = 8$. The covariance term is here negligible except at $x/D = 8$ where it slightly reduces the peak of turbulence at the top-left end of the wake. Term (VI) and

https://doi.org/10.5194/wes-2022-46
Preprint. Discussion started: 31 May 2022

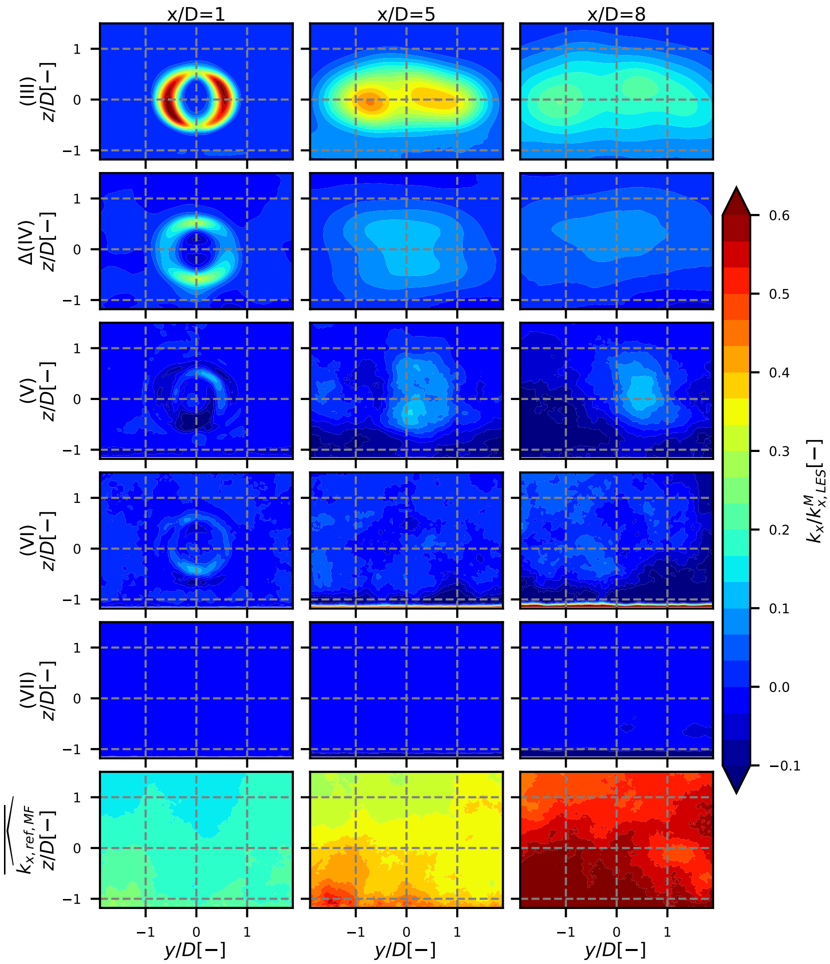

Figure 9. Same as 8 for the unstable case.

particularly term (VII) are negligible in front of the term (IV). The shape of all these terms is skewed due to the strong veer present in the stable ABL.

5.2 Physical interpretation

Term (III) or k_m is the pure meandering term. For a fixed point downstream the turbine, the meandering of the wake induces an alternation between low velocity (when the point is inside the wake) and high velocity (when it is outside the wake), i.e. variance in the unsteady velocity field, which is the definition of turbulence. k_m thus increases with the velocity deficit in the MFOR and with the amount of meandering. The former decreases with x whereas the latter increases with x, often linearly (Keck et al., 2013a; Ning and Wan, 2019; Brugger et al., 2022). These two contradictory trends lead k_m to be strong and very localised at the tip of the blades in the near wake and to be progressively smeared as the wake travels downstream. Since

https://doi.org/10.5194/wes-2022-46
Preprint. Discussion started: 31 May 2022

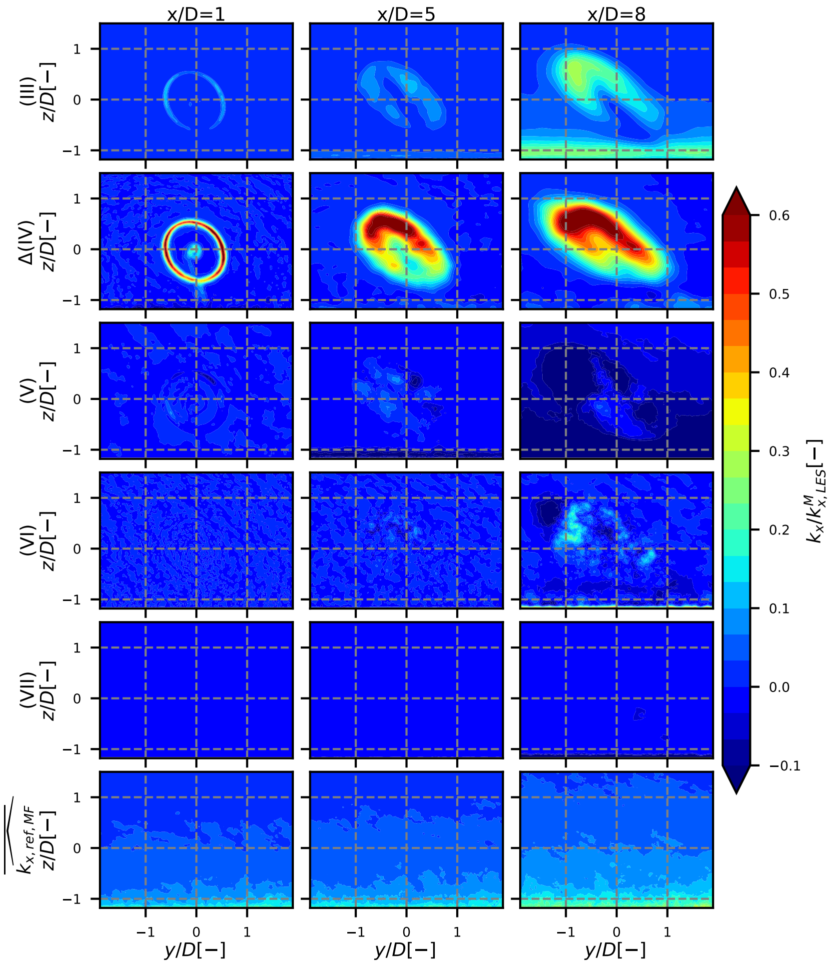

Figure 10. Same as 8 for the stable case.

the meandering is stronger in the horizontal direction than in the vertical direction and the velocity deficit is approximately axisymmetric (see the companion paper for more details), the highest values of k_m in the horizontal plane are stronger than in the vertical plane.

At a fixed x, the maximum values of k_m are localised near the tip of the blades in the near wake and are gradually spread as the wake travels downstream. The maximum added TI (i.e. square-root of the maximum value, normalised by the upstream velocity at hub height) induced by term (III) is plotted in dashed lines as a function of x/D in Fig. 11. As seen in Figs. 8,9 and 10, the meandering-induced turbulence is inversely related to the atmospheric stability, but this term also decreases faster in the unstable case, likely because the stronger the meandering, the more dissipated is the wake. Consequently, at $x/D = 8$ the unstable and neutral added TI due to the meandering are almost identical, and the curves would probably switch at larger x. In the stable case, the velocity profile is barely dissipated up to $x/D = 8$ and the meandering starts to take consequent values at

https://doi.org/10.5194/wes-2022-46
Preprint. Discussion started: 31 May 2022

$x/D = 5$, which results in an increase of the added turbulence due to meandering starting from $x/D = 5$. One can predict that beyond $x/D = 8$, a maximum value is reached, followed by a shape similar to the unstable and neutral case.

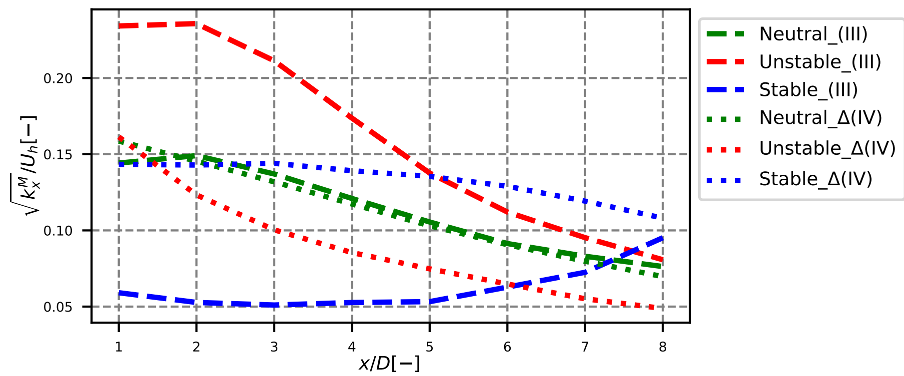

Figure 11. Evolution of the maximum value of terms (III) and Δ(IV) with x, normalized by the velocity at hub height.

Term Δ(IV) noted k_a for 'rotor added turbulence' is the turbulence that would exist in the wake of the turbine if there was no meandering. This turbulence is mainly due to the velocity gradient in the MFOR, localised at the edge of the wake. It is affected by the shear of the ABL, leading to a stronger gradient near the top tip and thus stronger rotor-added turbulence. This is particularly visible in the neutral and stable cases, where the atmospheric shear is significant. Similarly to the velocity field, this added turbulence is spread by meandering, more strongly in the lateral direction than in the vertical one, leading in the unstable case to lower values of k_a at the side tips than the bottom tip despite the atmospheric shear being stronger at the side. This spreading of meandering also induces lower values of maximum added turbulence for lower stability cases (dotted lines in Fig. 11). In order to analyse the shape of the rotor-added turbulence before the spreading due to meandering, one needs to look at the values of k_a in the MFOR. It is normalised with the hub height velocity to give the added TI in the MFOR:

$$\Delta TI_{MF} = \frac{|\Delta k_{x,MF}|}{\Delta k_{x,MF}} \cdot \frac{\sqrt{|\Delta k_{x,MF}|}}{U_h} \tag{24}$$

Equation 24 allows identifying in which region the turbulence in the MFOR is lower than the unperturbed turbulence, without leading to undefined values of the square root. The values of ΔTI_{MF} in the three cases of stability are plotted in Fig. 12 at different positions downstream.

First, it must be noted that the magnitude of the normalised added turbulence in the vicinity of the turbine (at $x/D = 1$) is very similar in all cases (between 15 % and 18 %), despite different values of atmospheric stability, shear and hub height velocity. At this position, the added turbulence in the MFOR is almost axisymmetric. Since the thrust coefficient and tip speed ratio are similar for the three cases, it seems acceptable for future model calibrations to suppose that Δk_{MF} is solely a function of the turbine regime. As the wake travels downstream, the asymmetry increases, in particular in the neutral and stable cases, but the magnitudes of ΔTI are still similar among the different cases. The asymmetry is attributed to the ambient shear, which increases with the stability. Negative values of Δk_{MF} are observed in the near wake between the wake centre and the edge

https://doi.org/10.5194/wes-2022-46
Preprint. Discussion started: 31 May 2022

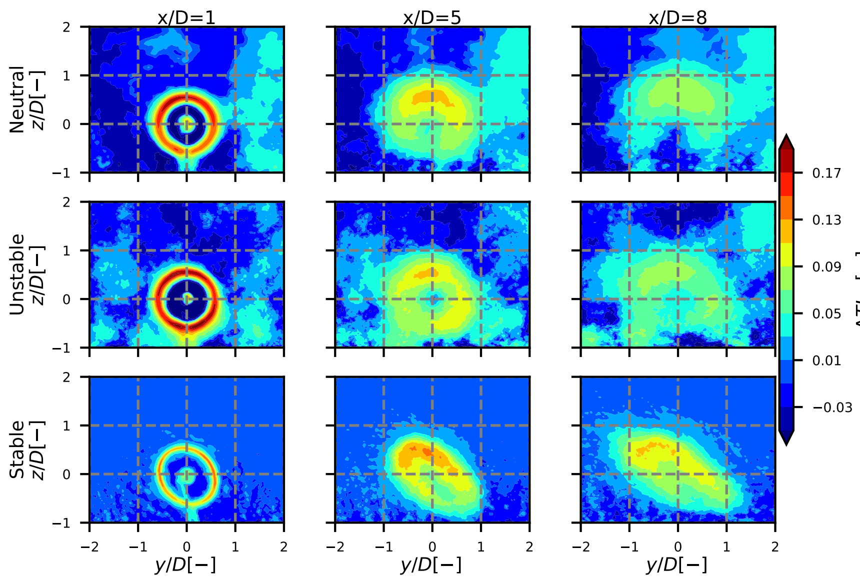

Figure 12. 2D map of the added turbulence in the MFOR, normalised by the velocity at hub height.

in the neutral and unstable cases and also in the bottom of the far wake in the neutral case. This indicates a transfer of energy from such regions to the high turbulence region, i.e. the edge and the top of the wake.

The value of the cross-terms (V), (VI) and (VII) is 0 either if there is no meandering (i.e. $\widehat{a} = a$) or if there is no turbulence in the MFOR ($U'_{MF} = 0$). Even though the latter can be assumed in some models, none of these conditions is fulfilled in real cases. It has been chosen to regroup the two terms $\overline{\widehat{\overline{U_{MF}}}\widehat{U'_{MF}}} - \overline{\widehat{\overline{U_{MF}}}}\,\overline{\widehat{U'_{MF}}}$ into one single covariance term (V) since those two terms were very large (in absolute value), compensating each other, and thus hard to interpret. Mathematically, this covariance term quantifies how the mean and varying parts of U_{MF} evolve together once displaced by the meandering operation $\widehat{\cdot}$. In the near wake, the non-zero values are distributed at the tip of the blades and then gradually expand in the whole wake. Negative and positive values are symmetrically distributed (along the horizontal and vertical axis for the neutral and unstable cases respectively). From these results, no physical interpretation nor a relation between the values of U_x or k_x in the wake with the term (V) could be found yet. Modelling the covariance term has thus not been achieved in the companion paper, but the authors are confident that it is important for a good wake model based on the meandering, and that it is reachable given the shapes observed in Figs. 8 and 9.

Term (VI) can be viewed as the varying part of turbulence: before being moved by the meandering and averaged, this term is the varying part of the square of the deviation from the mean (in opposition to $k_{a,MF}$ which is the mean part of the square of the deviation from the mean). In the near wake, positive values are present at the tip of the blades in the neutral and unstable cases, but also outside of the wake. It then gradually expands in the whole wake and seems randomly distributed in the wake region with negative and positive values. From Figs 8, 9 and 10, it seems that excepted systematic negative values near the ground

https://doi.org/10.5194/wes-2022-46
Preprint. Discussion started: 31 May 2022

($z < -0.5D$), this term mainly reproduces the spatial non-homogeneity of the wake and is thus not vital to be represented in an analytical model.

Term (VII) is always negative from its mathematical formulation: similarly to the viscous dissipation in the Navier-Stokes equations, it is a sink of energy. It has negligible values in all the stability cases. This last result should be taken with care: if the analogy with the viscous dissipation hold for this term, it means that it concerns small scales eddies, i.e. variations of the wind velocity at high frequency. Yet, as explained in Sect. 3, only the variations of time scale larger than 1 s are captured with the post-processing used in this work because of memory limitations. With a sampling frequency higher than 1 Hz, this term may have higher values.

It is important to note that all these results are sensitive to the wake tracking method: despite the method used here being among the most reliable available in the literature, there are always frames where the tracking failed, plus the limitations described in Sect. 3.5. For instance, the turbulence field in the MFOR (see Fig. 12) is noisier and noisier as the wake travels downstream and in particular in the unstable case, which can be interpreted as a consequence of the tracking algorithm being less and less reliable. This remark can be extended to all the terms of the turbulence equation presented in Figs. 8, 9 and 10. Moreover, the values and shapes of the different terms (in particular the cross-terms) might also change depending on the turbulence field, i.e. the eddies of the ABL, even for similar mean atmospheric conditions.

6 Conclusions and perspectives

In models predicting wake meandering such as the DWM, it is assumed that the turbulence in the wake can be separated into two parts: the turbulence generated by the rotor and the turbulence generated by meandering. In this work, the turbulence in the FFOR has been developed as a function of the two terms aforementioned and it appears that three cross-terms are missing, thus implicitly neglected in DWM-type models. A similar conclusion is drawn for the velocity, with one missing term.

To quantify the importance of each of these terms, and estimate the error induced by the assumptions of such models, LESs with actuator line are performed to model the wake of an isolated wind turbine inside an ABL. The modelled turbine is the modified Vestas V27 used in the SWiFT campaign of measurements, and three cases of atmospheric stability are investigated: near-neutral, unstable and strongly stable. The instantaneous wake centre is detected at different planes downstream of the turbine (from 1 D to 8 D) to compute the velocity field in the MFOR. The main conclusions are the following:

- Neglecting the cross-term of the mean velocity equation leads to small differences in the computation of the mean velocity profile in the FFOR. For the neutral case, the corresponding error leads to a less than 3 % overestimation of the available power in the wake of the wind turbine for a turbine located further than 2 D behind the wake emitting rotor.

- Neglecting cross-terms in the computation of turbulence in the FFOR leads to vertical profiles where the imbalance between the turbulence at the bottom tip and the top tip is underestimated. Adding the three missing cross-term allows to correct this error and drastically reduce the overall RMSE.

https://doi.org/10.5194/wes-2022-46
Preprint. Discussion started: 31 May 2022

– In the unstable case, the meandering term is dominating the total axial turbulence whereas in the stable case, it is the turbulence added by the rotor which is dominant. In the neutral case those two terms are of similar magnitude and overall larger than the cross-terms. These cross-terms, especially the so-called covariance term however show local values sufficiently strong to correct significantly the maximum axial turbulence in the wake.

It must be noted that these conclusions are drawn on the results of three particular cases of atmospheric stability and one model of turbine that can be regarded as rather small compared to modern rotors. The orders of magnitude given in this work should not be considered universal but are a good indication that for an accurate version of DWM-type models, the cross-terms (or at least the covariance term) must be taken into account. In the companion paper, an analytical model for the dominant terms is developed on the neutral and unstable cases presented herein.

Code and data availability. The code Meso-NH is open-source and can be downloaded on the dedicated website. The authors can provide the source code of the modified version 5-4-3 that was used in this work. The results of the LES simulations can also be directly provided.

Author contributions. EJ developed the equations, and performed the simulations with VM. All the authors worked on the interpretation of the results. The manuscript has been written by EJ with the feedbacks of FB and VM. The data used for the plot presented here and in part 1 are available under this online deposit: 10.5281/zenodo.6562720.

Competing interests. The authors declare that they have no competing interests.

https://doi.org/10.5194/wes-2022-46
Preprint. Discussion started: 31 May 2022

References

Abkar, M. and Porté-Agel, F.: Influence of atmospheric stability on wind-turbine wakes: A large-eddy simulation study, Physics of Fluids, 27, 035 104, https://doi.org/10.1063/1.4913695, 2015.

Ainslie, J. F.: Development of an eddy viscosity model for wind turbine wakes, in: 7th BWEA Wind Energy Conf., 1985.

Brugger, P., Markfort, C., and Porté-Agel, F.: Field measurements of wake meandering at a utility-scale wind turbine with nacelle-mounted Doppler lidars, Wind Energy Science, 7, 185–199, https://doi.org/10.5194/wes-7-185-2022, 2022.

Conti, D., Dimitrov, N., Peña, A., and Herges, T.: Probabilistic estimation of the Dynamic Wake Meandering model parameters using SpinnerLidar-derived wake characteristics, Wind Energy Science, 6, 1117–1142, https://doi.org/10.5194/wes-6-1117-2021, 2021.

Cuxart, J., Bougeault, P., and Redelsperger, J.-L.: A turbulence scheme allowing for mesoscale and large-eddy simulations, Quarterly Journal of the Royal Meteorological Society, 126, 1–30, https://doi.org/10.1002/qj.49712656202, 2000.

Deardorff, J. W.: Stratocumulus-capped mixed layers derived from a three-dimensional model, Boundary-Layer Meteorology, 18, 495–527, https://doi.org/10.1007/bf00119502, 1980.

Doubrawa, P., Quon, E. W., Martinez-Tossas, L. A., Shaler, K., Debnath, M., Hamilton, N., Herges, T. G., Maniaci, D., Kelley, C. L., Hsieh, A. S., Blaylock, M. L., Laan, P., Andersen, S. J., Krueger, S., Cathelain, M., Schlez, W., Jonkman, J., Branlard, E., Steinfeld, G., Schmidt, S., Blondel, F., Lukassen, L. J., and Moriarty, P.: Multimodel validation of single wakes in neutral and stratified atmospheric conditions, Wind Energy, https://doi.org/10.1002/we.2543, 2020.

Du, B., Ge, M., Zeng, C., Cui, G., and Liu, Y.: Influence of atmospheric stability on wind turbine wakes with a certain hub-height turbulence intensity, Physics of Fluids, https://doi.org/10.1063/5.0050861, 2021.

Jézéquel, E., Cathelain, M., Masson, V., and Blondel, F.: Validation of wind turbine wakes modelled by the Meso-NH LES solver under different cases of stability, Journal of Physics: Conference Series, 1934, 012 003, https://doi.org/10.1088/1742-6596/1934/1/012003, 2021.

Joulin, P.-A., Mayol, M. L., Masson, V., Blondel, F., Rodier, Q., Cathelain, M., and Lac, C.: The Actuator Line Method in the Meteorological LES Model Meso-NH to Analyze the Horns Rev 1 Wind Farm Photo Case, Frontiers in Earth Science, 7, https://doi.org/10.3389/feart.2019.00350, 2020.

Keck, R.-E., Maré, M. d., Churchfield, M. J., Lee, S., Larsen, G., and Madsen, H. A.: On atmospheric stability in the dynamic wake meandering model, Wind Energy, 17, 1689–1710, https://doi.org/10.1002/we.1662, 2013a.

Keck, R.-E., Maré, M. d., Churchfield, M. J., Lee, S., Larsen, G., and Madsen, H. A.: Two improvements to the dynamic wake meandering model: including the effects of atmospheric shear on wake turbulence and incorporating turbulence build-up in a row of wind turbines, Wind Energy, pp. n/a–n/a, https://doi.org/10.1002/we.1686, 2013b.

Lac, C., Chaboureau, J.-P., Masson, V., Pinty, J.-P., Tulet, P., Escobar, J., Leriche, M., Barthe, C., Aouizerats, B., Augros, C., Aumond, P., Auguste, F., Bechtold, P., Berthet, S., Bielli, S., Bosseur, F., Caumont, O., Cohard, J.-M., Colin, J., Couvreux, F., Cuxart, J., Delautier, G., Dauhut, T., Ducrocq, V., Filippi, J.-B., Gazen, D., Geoffroy, O., Gheusi, F., Honnert, R., Lafore, J.-P., Brossier, C. L., Libois, Q., Lunet, T., Mari, C., Maric, T., Mascart, P., Mogé, M., Molinié, G., Nuissier, O., Pantillon, F., Peyrillé, P., Pergaud, J., Perraud, E., Pianezze, J., Redelsperger, J.-L., Ricard, D., Richard, E., Riette, S., Rodier, Q., Schoetter, R., Seyfried, L., Stein, J., Suhre, K., Taufour, M., Thouron, O., Turner, S., Verrelle, A., Vié, B., Visentin, F., Vionnet, V., and Wautelet, P.: Overview of the Meso-NH model version 5.4 and its applications, Geoscientific Model Development, 11, 1929–1969, https://doi.org/10.5194/gmd-11-1929-2018, 2018.

https://doi.org/10.5194/wes-2022-46
Preprint. Discussion started: 31 May 2022

Lafore, J. P., Stein, J., Asencio, N., Bougeault, P., Ducrocq, V., Duron, J., Fischer, C., Héreil, P., Mascart, P., Masson, V., Pinty, J. P., Redelsperger, J. L., Richard, E., and de Arellano, J. V.-G.: The Meso-NH Atmospheric Simulation System. Part I: adiabatic formulation and control simulations, Annales Geophysicae, 16, 90–109, https://doi.org/10.1007/s00585-997-0090-6, 1998.

Larsen, G., Pedersen, A., Hansen, K., Larsen, T., Courtney, M., and Sjöholm, M.: Full-scale 3D remote sensing of wake turbulence - a taster, Journal of Physics: Conference Series, 1256, 012 001, https://doi.org/10.1088/1742-6596/1256/1/012001, 2019.

Larsen, G. C., Madsen, H. A., Thomsen, K., and Larsen, T. J.: Wake meandering: a pragmatic approach, Wind Energy, 11, 377–395, https://doi.org/10.1002/we.267, 2008.

Madsen, H. A., Larsen, G. C., Larsen, T. J., Troldborg, N., and Mikkelsen, R.: Calibration and Validation of the Dynamic Wake Meandering Model for Implementation in an Aeroelastic Code, Journal of Solar Energy Engineering, 132, https://doi.org/10.1115/1.4002555, 2010.

Ning, X. and Wan, D.: LES Study of Wake Meandering in Different Atmospheric Stabilities and Its Effects on Wind Turbine Aerodynamics, Sustainability, 11, 6939, https://doi.org/10.3390/su11246939, 2019.

Quon, E. W., Doubrawa, P., and Debnath, M.: Comparison of Rotor Wake Identification and Characterization Methods for the Analysis of Wake Dynamics and Evolution, Journal of Physics: Conference Series, 1452, 012 070, https://doi.org/10.1088/1742-6596/1452/1/012070, 2020.

Stein, J., Richard, E., Lafore, J. P., Pinty, J. P., Asencio, N., and Cosma, S.: High-Resolution Non-Hydrostatic Simulations of Flash-Flood Episodes with Grid-Nesting and Ice-Phase Parameterization, Meteorology and Atmospheric Physics, 72, 203–221, https://doi.org/10.1007/s007030050016, 2000.

Stevens, R. J., Martínez-Tossas, L. A., and Meneveau, C.: Comparison of wind farm large eddy simulations using actuator disk and actuator line models with wind tunnel experiments, Renewable Energy, 116, 470–478, https://doi.org/10.1016/j.renene.2017.08.072, 2018.

Sørensen, J. N. and Shen, W. Z.: Numerical Modeling of Wind Turbine Wakes, Journal of Fluids Engineering, 124, 393–399, https://doi.org/10.1115/1.1471361, 2002.

Troldborg, N.: Actuator Line Modeling of Wind Turbine Wakes, PhD Thesis, 2009.